The Space Debris Sensor Experiment

P. Anz-Meador[1], M. Ward[1], A. Manis[2], K. Nornoo[1], B. Dolan[1], C. Claunch[3], J. Rivera[3]

[1]Jacobs, NASA Johnson Space Center, Mail Code XI5-9E, 2101 NASA Parkway, Houston, TX 77058, USA, phillip.d.anz-meador@nasa.gov
[2]HX5 – Jacobs JETS Contract, NASA Johnson Space Center, Mail Code XI5-9E, 2101 NASA Parkway, Houston, TX 77058, USA
[3]GeoControl Systems – Jacobs JETS Contract, NASA Johnson Space Center, Mail Code XI5-9E, 2101 NASA Parkway, Houston, TX 77058, USA

ABSTRACT

The Space Debris Sensor (SDS) is a NASA Class 1E technology demonstration external payload aboard the International Space Station (ISS). With approximately one square meter of detection area, the SDS is attached to the European Space Agency Columbus module facing the ISS velocity vector with minimal obstruction from ISS hardware. The SDS is the first flight demonstration of the Debris Resistive/Acoustic Grid Orbital NASA-Navy Sensor (DRAGONS) technology developed and matured over 10 years by the NASA Orbital Debris Program Office (ODPO), in concert with the DRAGONS consortium, to provide information on the sub-millimeter scale orbital debris environment. The SDS demonstrated the capacity to read 4 resistive grids at 1 Hz, 40 acoustic sensors at 500 kHz, and record and downlink impact data to the ground. Observable and derived data from the SDS could provide information to models that are critical to understanding risks the small debris environment poses to spacecraft in low Earth orbit. The technology demonstrated by the SDS is a major step forward in monitoring and characterizing the space debris environment. This paper will address the technical performance of the SDS during its operational lifetime and its realization of technical and scientific goals. The SDS was intended to operate for 3 years; however, the payload incurred multiple anomalies during its operational life. Subsequently termed "Anomaly #1," the first was the symptomatic loss of low data rate 1553 channel command and telemetry. The second, Anomaly #2, was loss of all low- and medium-data rate (Ethernet) telemetry. Anomaly #2 proved to be unrecoverable, leading to loss of the payload after approximately 26 days on-board the ISS. Therefore, this paper also addresses the anomalies that occurred during operation of the SDS, their attribution, and their resolution. Lessons learned are described when relevant to anomaly identification, attribution, and resolution.

1 OVERVIEW & TECHNOLOGY DEMONSTRATION

The Space Debris Sensor (SDS) is a National Aeronautics and Space Administration (NASA) Class 1E technology demonstration external payload aboard the International Space Station (ISS) [1]. The SDS was the first flight demonstration of the Debris Resistive/Acoustic Grid Orbital NASA-Navy Sensor (DRAGONS) technology developed and matured by the NASA Orbital Debris Program Office (ODPO). In collaboration with the Naval Research Laboratory, the U.S. Naval Academy, and the University of Kent, the DRAGONS sensor was created to provide information on the orbital debris population that is too small for ground-based remote sensing. The SDS payload was required to operate for a minimum of 2 years, detect impacts larger than 50 μm, and record impact time and location as well as projectile direction, speed, and size. It consisted of three layers, the first a resistive grid layer to detect impacts and infer debris particle sizes, the second an unpowered grid, and the third a solid backstop to measure impact energy. All three layers had acoustic sensors to detect impact times and locations. The first and second layers had 16 acoustic sensors each, and the third layer had 8, for a total of 40. The time of impact on sequential layers provides a measure of the relative velocity of an impacting particle. The energy on the backstop would provide a measure of the particle density. SDS demonstrated the technology required to read and record 4 resistive grids at 1 Hz, 40 acoustic sensors at 500 kHz, and downlink impact data to the ground. The daily 1 Hz data consisted of a counter of impacts recorded, ISS state vector and attitude, resistance values, temperatures for each of the 10 acoustically distinct areas, and voltage readings from each acoustic sensor. When triggered by an acoustic sensor reading above a set, user-configurable threshold, the SDS recorded 2.5 ms of data. SDS data was recorded in three types of files: acoustic, compact reconfigurable input/output (RIO) and single-board RIO controllers (cRIO and sbRIO) data, and health and status (H&S) files. When commanded from the ground, data were downlinked to the NASA Payload Operations and Integration Center.

The SDS was launched to the ISS inboard the trunk of the Space-X Dragon vehicle on 15 December 2017 and was installed on the Columbus module of the ISS on 1 January 2018. The SDS collected over 1200 acoustic detection files, approximately 26 days of resistance/engineering data, and demonstrated impact detection in the flight environment. Unfortunately, shortly after the beginning of operations, the SDS began experiencing anomalous behavior, and after approximately 26 days, became unresponsive. Due to its prematurely terminated mission, the SDS failed to operate over a 2-year time interval, observe an acknowledged impact on the backstop layer, and resolve projectile mass density from impact energy delivered to the backstop. Despite its short operational lifetime, the SDS mission was a success in detecting impacts and determining impact time and location. The SDS technology demonstration scorecard is provided in Table 1. Impact time and location was successfully demonstrated, evident by the over 1200 triggered events recorded in the acoustic data stream. The projectile direction, speed, size, and density could not be characterized due to there being no valid impacts on the second and third layers, and no correlation between gridline severs and acoustic events, which resulted in 'fail' scores. However, environmental data and the SDS performance continue to inform the development of other operational *in situ* sensors.

Table 1. SDS Technology Scorecard. Green = pass, red = fail.

Component	Ground testing	Flight experience
Impact Detection	P	P
Impact time	P	P
Impact location	P	P
Projectile direction	P	F
Projectile speed	P	F
Projectile size (via grid line severance)	P	F
Projectile density (via impact energy)	P	F

2 MMOD MEASUREMENT

The dual goals of the SDS were to update the micrometeoroid and orbital debris (MMOD) environment definition from a scientific perspective and conduct a technology demonstration. Analysis of SDS science data suggests it is consistent with the ISS-altitude MMOD environment for the short area-time product. The Hypervelocity Impact Technology (HVIT) group performed MMOD impact risk assessments using the BUMPER II finite element-modeling program [2] for the SDS 2018-2020 installation, which uses NASA's latest Meteoroid Engineering Model (MEM-R2 [3]) and Orbital Debris Engineering Model (ORDEM 3.0 [4]). Results of the BUMPER II modeling is shown in Fig. 1, scaled to the estimated sensor uptime of 22.12 days. White Sands Test Facility (WSTF) ground testing demonstrated that the SDS successfully detected 50 µm projectiles at 7 km/s and this is indicated by the vertical dashed line in the figure. Five valid impacts were recorded by SDS, and these appear consistent with the expected number of impacts down to this approximate detection threshold.
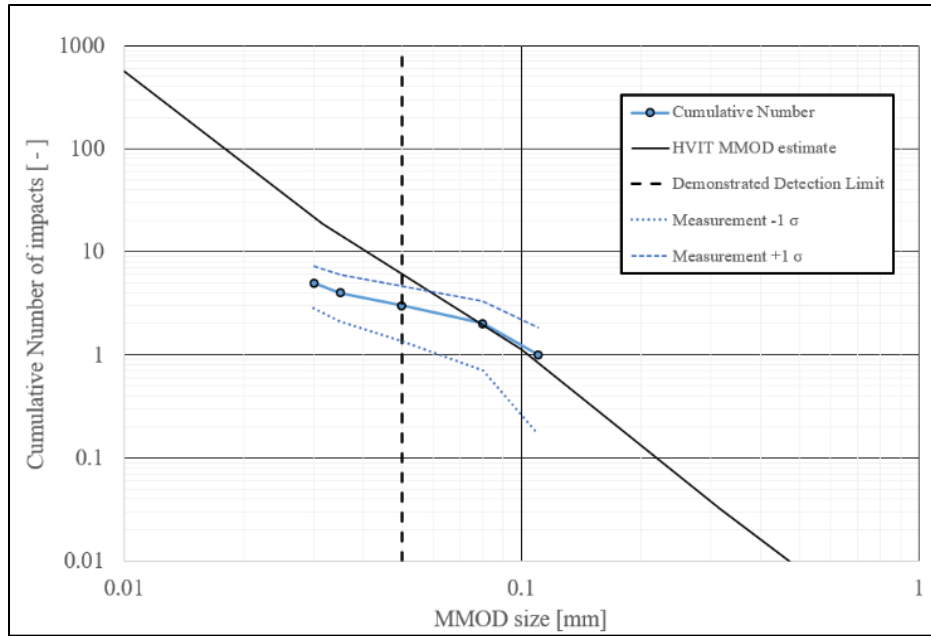
Fig. 1. SDS valid measurements compared to Bumper II total environment prediction.

In Fig. 1, projectile sizes were estimated by a relationship derived in WSTF testing between peak acoustic signal strength and projectile size; actual particle size is less than or equal to that portrayed in the figure. This relationship was demonstrated with sufficient accuracy to apply in lieu of grid line breaks. No grid line breaks were associated with acoustically triggered events on orbit. This is not unexpected given the short operational SDS lifetime and the preponderance of smaller MMOD in power law models of the environment.

3   SCIENCE DATA APPLICATIONS

3.1   Resistance Data

A resistance change on the SDS grid indicated a resistance grid line broken, from which the impact hole size can be estimated (and therefore particle size) based on damage models derived from hypervelocity testing. It was observed the first few days after installation aboard the ISS that SDS displayed a "burn-in" effect change in resistance on all resistive subgrids, which stabilized after approximately a week. Figure 2 illustrates an example of the beginning "burn-in" effect followed by stabilization for a resistor with change in time. More generally, resistance displayed a regular, repeating pattern as the temperature varied, as shown in Fig. 3.
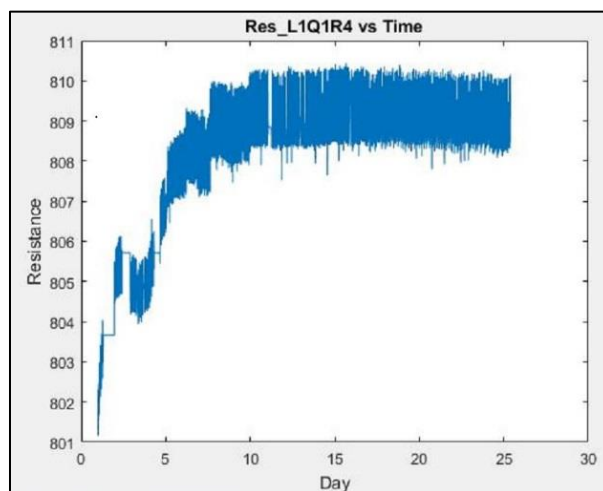

Fig. 2. Typical SDS subgrid resistance behavior over operational lifetime (2018-day number). Note burn-in period.
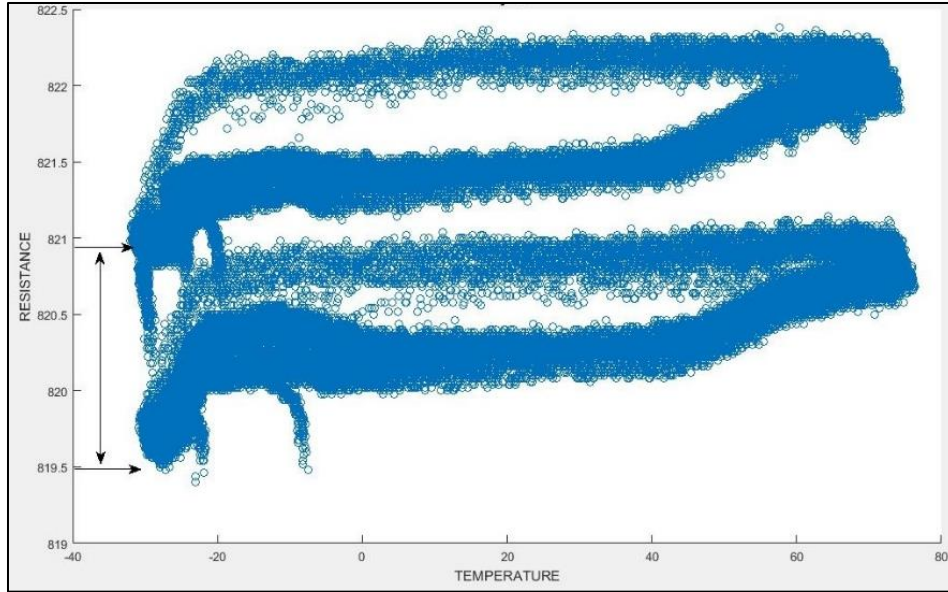
Fig. 3. Example of a resistor's response to cyclic temperature changes and an irreversible change of approximately 1.5 Ω. This change in resistance is consistent with the breaking of one grid line.

Potential impacts were identified as a resistance change (1 ohm [Ω] or more) over each resistor. There were approximately 27 instances of this behavior over the course of operation of the SDS. The 27 potential impacts were normalized to their first recorded resistance in each resistor time interval (when the resistance change became greater than 1Ω). Figure 4 illustrates each identified resistor with a resistance change greater than 1Ω over a time interval.
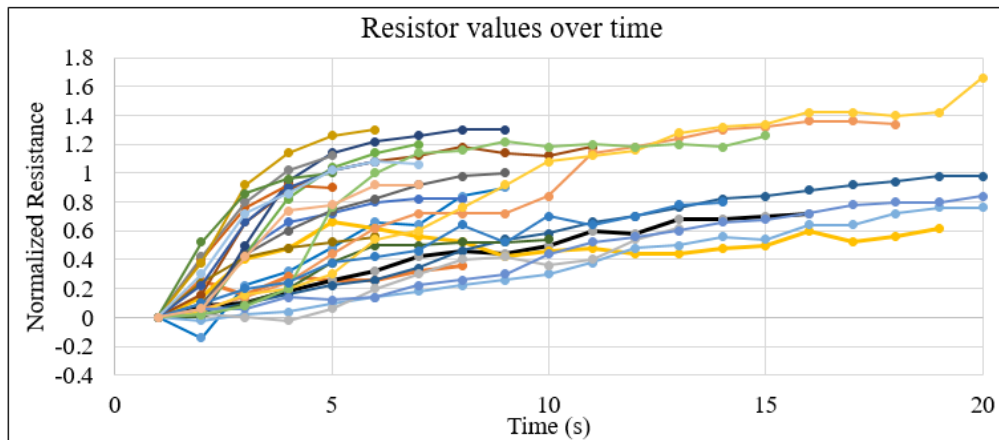

Fig. 4. Twenty-seven resistor behaviors over time.

Two different modalities of resistance change were observed. The behavior is separated based on the duration of resistance change and the length of time that elapsed between the 1Ω changes. Characterized as either a slow "S" curve or a "prompt" jump in resistance (top two charts in Fig. 5, respectively), the latter would be expected in the case of an impact-induced sever, and is consistent with SDS grid ground testing (bottom chart in Fig. 5). The time interval from which the "S" curve changes resistance does not follow ground testing's instantaneous resistance change for an impact. Ground testing produced an immediate 1Ω jump in resistance, while the "S" curve resistor behavior on average lasted 20 seconds. The phenomenology of the "S" events is not understood at this time, but it is unlikely to be associated with an impact.
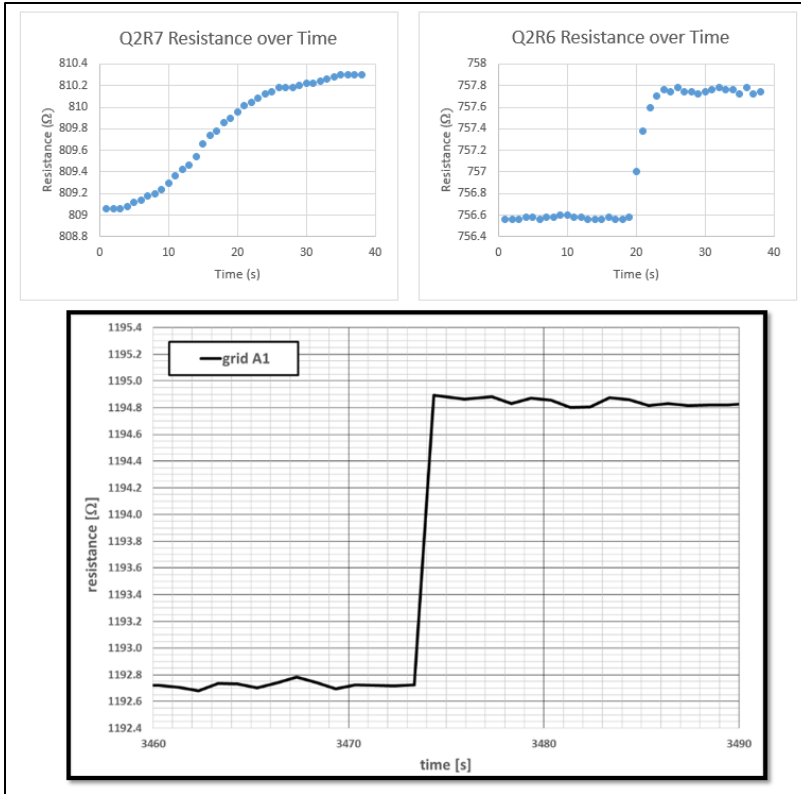
Fig. 5. SDS Resistor behavior on orbit (top) and ground testing resistor behavior (bottom).

3.2 Acoustic Data

Acoustic sensors were placed on the SDS with the goal of detecting impact-induced acoustic waves in the grid's Kapton substrate. The SDS produced 1287 recoverable acoustic data files during its operation (some acoustic files were lost prior to downlink due to the circumstances of SDS anomalous behavior). Observed acoustic irregularities occurred during operation such as radio frequency (RF) flash, electromagnetic interference (EMI) signals, and signals being recorded in only one sensor (A), quadrant (Q), or layer (L). Due to the complexity of these signals and to expedite the impact detection process, acoustic files were classified into five categories (Table 2). A flowchart of the classification process is additionally provided in Fig. 6.

Table 2. Classifications of acoustic files.

| Identification	Characteristics
EMI	Signal appearing first on L3, wave packet shaped, constant wave pattern, or file created by noisy sensor.
One Sensor Response	Only showing signal on one sensor and in one quadrant and layer.
Flash	Large impulse signal showing simultaneously on multiple sensors, directly followed by flat line.
Probable Sensor Malfunction	Discontinuities of sensor output, or signal indicating instantaneous jump from negative to positive voltage.
Potential Acoustic Response	All else not classified as above. Time delays are consistent with expected acoustic travel time (from ground testing), large, low frequency impulse signals that are well defined and located. Observed in multiple layers, quadrants, and sensors.
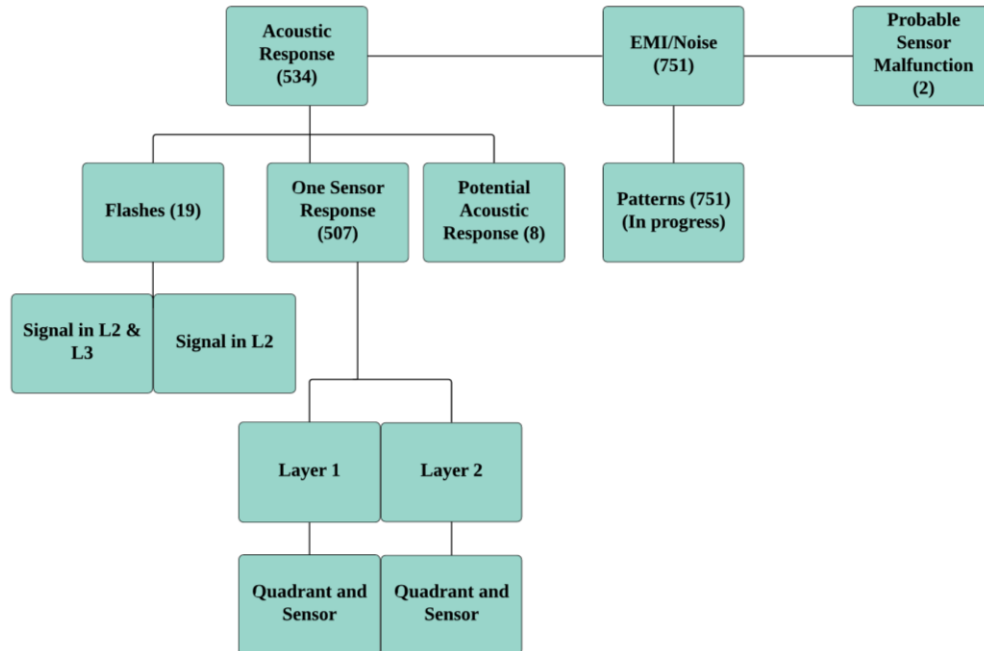
Fig. 6. SDS acoustic file classification process.

Of the acoustic files created, approximately 58% were EMI files, 40% were one-sensor response, 1.5% were flash response, and less than 1% were sensor malfunction and potential acoustic responses. After removing EMI and sensor malfunction types, 534 acoustic files were left. The SDS did not incur any impact penetrations through three grid layers, thus preventing the determination of impactor relative velocity and mass density. Seven candidate impacts were left that matched the acoustic response characteristics described in Table 2. These candidates were additionally analyzed by an acoustic signal subject matter expert with the conclusion that all files in Table 3 excepting #1226 were most likely an impact event, leaving the candidate impact total at six. One impact (#617) was omitted from both further analysis and Fig. 1 (estimated size well below 30 μm, the programmatic threshold of interest), leaving five valid impacts.

Table 3. SDS impact candidates, date/time impacted, and estimated maximum impactor size.

Acoustic File	Day	Time	Sensor Threshold (V)	Estimated Particle Size (μm)
593	7	04:10:09	.03	50
617	7	08:37:11	.03	< 12
993	11	01:17:09	.03	35
1097	14	05:44:49	.06	80
1120	18	07:27:15	.06	110
1172	20	17:31:28	.06	30
1226	22	15:30:39	.06	-

4   Anomaly Resolution

The SDS payload experienced H&S lockups beginning shortly after its installation on 1 January 2018. Termed "Anomaly #1" in retrospect, this anomaly resulted in the SDS no longer sending H&S data or responding to commands over the 1553-standard low data rate channel. Commanded hard power recycles provided a temporary work-around to clear the 'locked-up' state and restore the payload to nominal operation. Three weeks into operation, the SDS did not recover from three consecutive power recycle attempts to cope with Anomaly #1, and the payload failed to send any data or accept commands on either the 1553 low-data rate channel or the medium-data rate Ethernet channel. This failure to respond was termed "Anomaly #2." Additional power cycles were also

unsuccessful, and the payload was placed in a "safe" state with heater (direct current DC/DC converter) power on and operational (cRIO) power off. While never logged as a formal payload anomaly, SDS heater string performance (as indicated by DC/DC converter power draw) was also compromised. The heater's off-nominal performance was detected only during the electrical/amperage draw analysis performed while troubleshooting Anomalies #1 and #2. Observed power draw was consistent with only one of the two heater strings being functional. SDS staff referred to this condition colloquially as "Anomaly #3." As ISS orbital and configuration parameters, including payload insolation and the single heater string, were sufficient to maintain SDS environmental conditions in its nominal operating temperature range, emphasis was placed on resolving Anomalies #1 and #2. Anomalies #1 and #2 were formally reported in the NASA Payload Anomaly Reporting tool. Since Anomaly #3 did not impact payload operations, it was not formally reported. For a more thorough description of the SDS anomaly attribution, see [5]. Environmental effects and conditions, which could possibly interfere with SDS operational functionality, were analyzed as part of the anomaly resolution process and are discussed in the following section.

4.1   Environmental Effects

Environmental effects such as temperature, geographic location, space radiation, and trapped particles were all analyzed for correlating with lockups of the SDS, but also facilitated an exploration into the orbital environment of the ISS and SDS technologies. After an observed "burn-in" effect for the first week of SDS operation, the SDS cRIO temperature did not experience significant deviation from the average temperature. SDS thermal management was composed of thermostats and dual Kapton film heater strings. The heaters were powered during ascent and on-orbit storage in the Space-X Dragon trunk by the trunk's power distribution system and by the ISS after installation. Certain irregularities with regard to expected power draw were noted when powered either inboard the Dragon trunk or on-orbit. The working hypothesis is that after the heater turned on on-orbit, the resulting thermal expansion caused it to disconnect because the connection was already loose (Anomaly #3). The SDS temperature fell to ambient (day/night cycle, beta angle) heating and concomitant temperatures when unpowered. However, the temperatures never fell below -16 C (with the lower operational limit at -40 C). Geographic and environmental effects (ISS-local, orbital, etc.) on SDS behavior were examined. The beta angle (proportional to the percentage of time the object spends in direct sunlight) at which the ISS was positioned was considered (Fig. 7). After adjusting for time the SDS spent at each beta angle, there appears to be no effect of beta angle on the SDS, and it is unlikely there is a relationship between the number of lockups and beta angle.
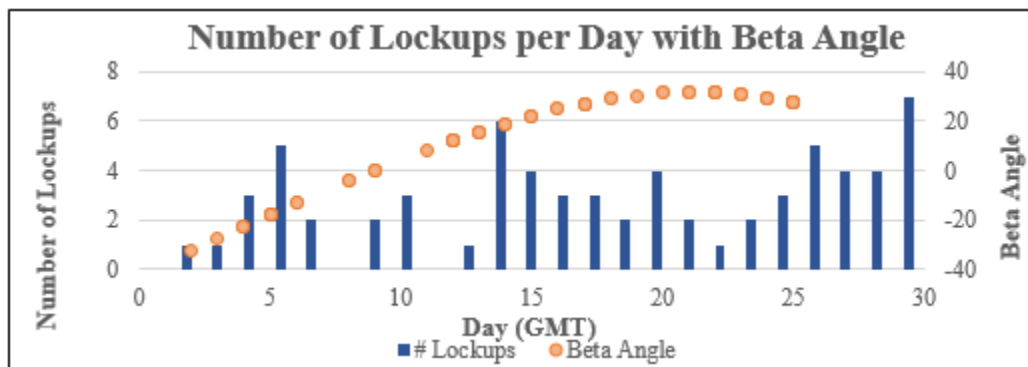

Fig. 7. The number of lockups that occurred each day on the SDS charted with the daily Beta angle.

The SDS environmental effects investigation continued with observation of lockup occurrences at calculated orbital dawns. Figure 8 displays the lockups associated with a position of the ISS at orbital dawn. One lockup was correlated to orbital dawn but was interpreted as random chance, with no fundamental correlation of SDS lockups to orbital dawn.
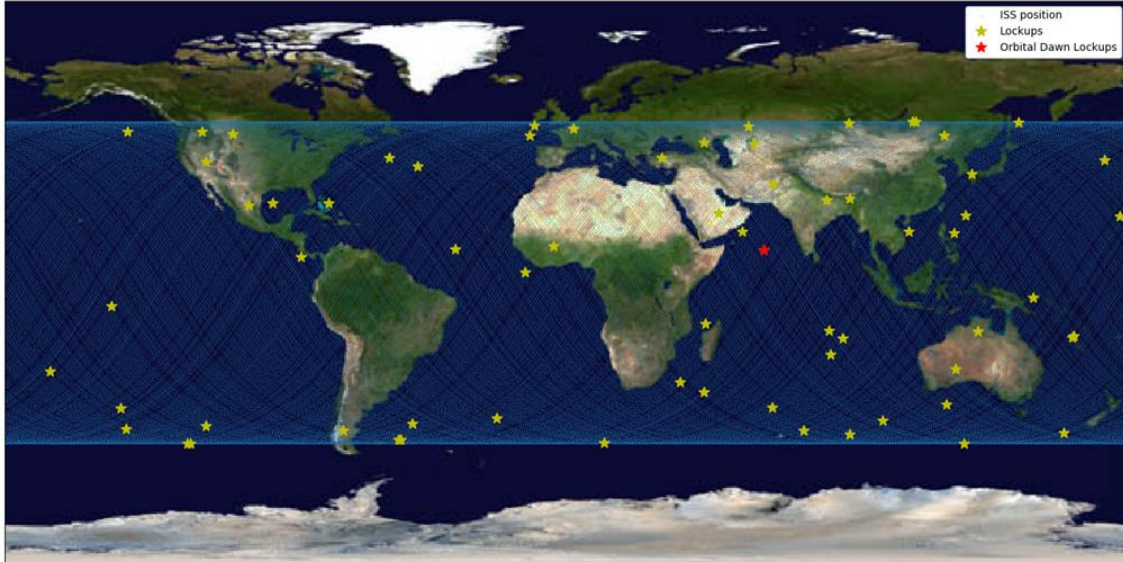
Fig. 8. Location of the ISS during lockup occurrences (yellow) and orbital dawn associated lockup (red).

Another consideration is Earth-fixed coordinates (latitude-longitude of sub-satellite point, altitude above geoid) of lockups, and any possible correlation with the South Atlantic Anomaly (SAA) or ground-based space surveillance radars. The latitude and longitude coordinates of the SDS during lockups were compared to observe any occurrences of geographic position influence of the SDS. The total number of lockups was tallied into latitude ranges. The dependence on time in orbit at outermost latitudes was removed by using the Kessler function [6]. There was an uneven distribution of lockup occurrences, with a higher number of lockups occurring above the equator in the northern latitudes (Fig. 9).To formally test this hypothesis, a non-parametric test (Kolmogorov-Smirnov, [7]) of the equality of lockups to latitude distribution was executed. There was sufficient evidence to suggest the data does not follow a uniform distribution, and it was inferred that the lockup occurrences have a minor relationship to latitude position. However, this relationship was not significantly different enough from a random distribution to be considered a cause of the lockup behavior.
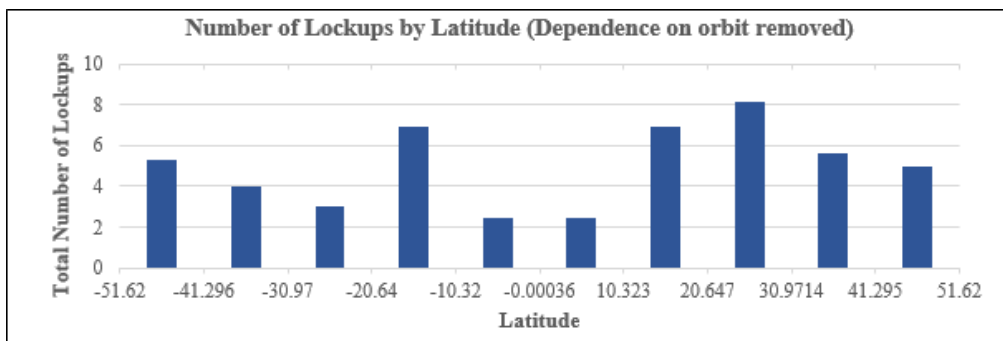

Fig. 9. Number of lockup occurrences and the Earth-fixed coordinates at which they occurred.

Other environmental components analyzed include relatively low-energy solar cosmic rays (SCRs), protons, and heavier ions; galactic cosmic rays (GCRs), produced by active galactic nuclei, and – internal to the Milky Way galaxy – supernovae and other energetic events and phenomena; and trapped particles (protons and electrons, including the SAA). During SDS' operational lifetime, there were no coronal mass ejections (proton rich) recorded, no X-ray flare events, nor reported SCR/GCR events. Solar weather, due to the solar wind and Earth magnetospheric particle ingestion, correlates with a disturbed geomagnetic field; this was examined for January 2018 to cover SDS' operational lifetime. A comparison of geomagnetic indices with number of lockups per day is shown in Fig. 10. No correlations are observed between the two variables.
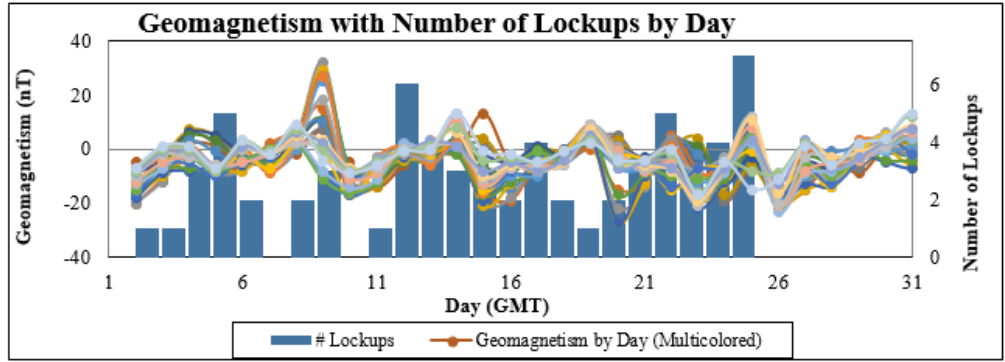
Fig. 10. Number of lockup occurrences compared with daily geomagnetism indices.

EMI and electromagnetic compatibility (EMC) were explored due to the large number of acoustic EMI files created. The geographic location of EMI file creation was charted and associated with lockups (Fig. 11). EMI/EMC at ISS altitude does not appear to be a probable contributing factor in lockups.
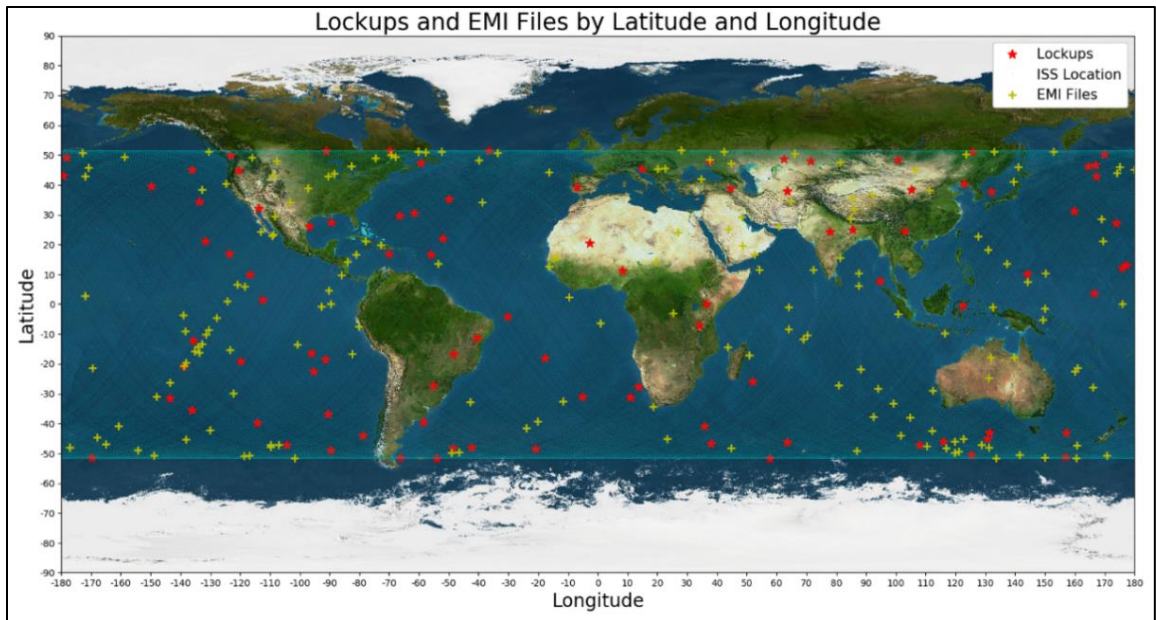

Fig. 11. EMI files and lockup occurrences.

Several unresolved correlations remain between SDS performance and ISS local or global environments. A number of SDS acoustic sensors exhibit long period (hours to days) noise phenomena; there appear to be several "beat" phenomena experienced by an otherwise quiet, nominally operating sensor (Fig. 12).While currently unexplained, science data analysis will attempt to identify and characterize this phenomenon further, including an estimate of noise frequency.
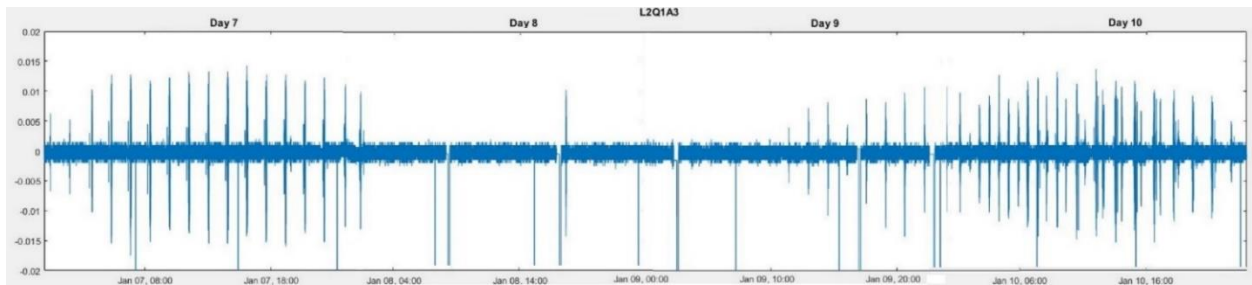

Fig. 12. Acoustic Sensor 3 recording of beat phenomena over a 3-day period.

4.2   Lessons Learned and Extensions to other Flight Profiles

SDS mission experience and lessons learned were carefully documented to maximize team success in future missions of *in situ* sensors. The SDS mission teams (Engineering and Operations) compiled these during the anomaly resolution and payload recovery effort, and documented them in a formal root cause analysis and anomaly resolution report. Areas of consideration for root cause assessment were the system architecture, sensors, electronic box, verifications, science data, and documentation. Overall, the environmental analysis indicated there was no clear relationship to either of the anomalies excepting a slight dependence on latitude. Anomaly #1 was attributed to a cRIO-sbRIO communications thread interruption, and the most probable cause of Anomaly #2 was determined to be a hardware failure of the boot sector-memory storage on the cRIO processor. While the environmental analysis was initiated in an effort to address Anomaly #1, all science data and lessons learned from the SDS mission directly assists other sensor and flight profiles in development.

5   Conclusions

SDS is a technology demonstrator flight payload developed under the NASA Class 1E program for experimental spaceflight hardware that demonstrated MMOD environmental measurements. The mission was hindered by reduced operational uptime and the unrecoverable loss of the payload after approximately 26 days onboard the ISS. Nonetheless, observable and derived science data from the SDS provided sensor technology for *in situ* MMOD environmental measurements and demonstrated consistent results with the ORDEM 3.0 and MEM-R2 environmental models for understanding risks that the small debris environment poses to spacecraft at the ISS altitude. Following the analysis of SDS-derived data, there are no likely relationships (other than slight latitude bias) between Anomaly #1 lockups and resistance, temperature, beta angle, orbital dawn, space weather/radiation effects, or EMI/EMC. The anomalies were determined to originate from file writing and memory storage errors. Currently, SDS is being prepared for disposal aboard the commercial resupply *Cygnus* vehicle Northrup-Grumman Number 12. During this process, the SDS sensor and electronics box module's surfaces are to be inspected for MMOD impact using ISS on-board high-resolution video. These may further inform both technology demonstration and science applications for other sensors and flight profiles.

6   REFERENCES

1. Hamilton, J., Liou, J.-C., Anz-Meador, P.D., *et al*. "Development of the Space Debris Sensor," presented at the 7th European Conf. Space Debris, April 2017. Available at https://conference.sdo.esoc.esa.int/proceedings/sdc7/paper/965. Accessed 30 September 2019.

2. Hyde, J.L., E.L. Christiansen, D.M. Lear, *et al*. "Overview of Recent Enhancements to the BUMPER-II Meteoroid & Orbital Debris Risk Assessment Tool," IAC-06-B6.3.03. Available at https://ntrs.nasa.gov/archive/nasa/casi.ntrs.nasa.gov/20060047566.pdf. Accessed 2 October 2019.

3. Moorhead, A.V, Koehler, H.M., and Cooke, W.J. "NASA Meteoroid Engineering Model Release 2.0," NASA/TM-2015-218214, October 2015.

4. Stansbery, E.G., Matney, M.J., Krisko, P.H., *et al*. "NASA Orbital Debris Engineering Model ORDEM 3.0 – Verification and Validation," NASA/TP-2015-218592, October 2015.

5. Matney, M. and Anz-Meador, P. "Space Debris Sensor Anomaly Attribution Scenario," 2018. Available at https://ntrs.nasa.gov/archive/nasa/casi.ntrs.nasa.gov/20050189209.pdf. Accessed 23 August 2019.

6. Kessler, D. "Derivation of the Collision Probability between Orbiting Objects: The Lifetimes of Jupiter's Outer Moons," ICARUS, Vol. 62, p. 46, 1981.

7. Chakravarti, I.M., Laha, R.G., and Roy, J. Handbook of Methods of Applied Statistics, Volume I, John Wiley and Sons, pp. 392-394, 1967.